ELSEVIER

Contents lists available at ScienceDirect

Scripta Materialia

journal homepage: www.journals.elsevier.com/scripta-materialia





In-situ investigation of tension-compression **asymmetry** of Ni-SiOC nanocomposites

Bingqiang Wei, Wenqian Wu, Jian Wang

Mechanical & Materials Engineering, University of Nebraska-Lincoln, Lincoln, NE 68588, USA

ARTICLE INFO

Keywords: Ni-SiOC nanocomposite Tension-compression asymmetry Strength plasticity

ABSTRACT

Ni-SiOC nanocomposites are synthesized through co-sputtering Ni and Si-O-C and then annealed at high temperature up to 800 °C to obtain two characteristic microstructures, core (crystalline Ni)-shell (amorphous ceramic SiOC) nanostructures and submicron-grained Ni containing amorphous ceramic SiOC particles. *In-situ* scanning electron microscope (SEM) compression tests show that both types of Ni-SiOC nanocomposites exhibit high strength and good plastic flow stability due to microstructure-promoted plastic co-deformation between amorphous ceramics and Ni grains. However, *in-situ* tension tests reveal that the core-shell nanostructures exhibit brittle fracture behaviour at a low strength due to cracking along amorphous cores, while the submicron-grained Ni can reach the similar strength to that of compression but a limited plasticity due to interface decohesion facilitated by deformation incompatibility between Ni and amorphous ceramic SiOC.

Strength, plastic flow stability and ductility of materials are highly dependant on their microstructures [1–3]. Ultra-fine and nano-grained materials [4–6] corresponding to grain boundary strengthening and nano-particles reinforced nanocomposites [7–9] corresponding to dispersion and precipitation strengthening mechanisms have been demonstrated to achieve high strength. However, microstructural stability and plastic flow stability are facing great challenge. For example, nanocrystalline (NC) metals present both limited plasticity and ductility due to easy onset of shear localization along grain boundaries (GBs) and low strain hardening capability of nanograins [10–12]. In addition, mechanically and/or thermally driven grain coarsening results in softening behaviour [13–15]. More seriously, the collective motion of grain boundaries may facilitate strain localization or shear banding in NC metals, producing plastic instability and poor ductility [16–18].

Retaining the microstructure of ultra-fine and nano-grained materials during mechanical and/or thermal loading could be realized through forming amorphous grain boundaries and/or secondary phases along grain boundaries [19–22]. Metallic glass (MG) grain boundaries have been demonstrated to improve strength and plasticity of NC alloys because nanoscale metallic glass layers exhibit high plastic flow [23–25]. For example, Cu based nanocrystalline-amorphous nanolaminates exhibit high flow strength and tensile ductility [23]. Core (Al nanograins) – shell (nanosized MG) nanostructures exhibit excellent compression strength (1.7 GPa) and plasticity (80%) [25]. Also, large

sized or bulk crystal-amorphous nanocomposites were reported to be fabricated via advanced laser processing [22] or melting spinning [26] techniques with extremely high cooling rates. However, metallic glass will recrystallize during plastic deformation and heating due to the low thermal stability [27]. Recently, nanograined Ni and amorphous ceramic SiOC form crystal-amorphous core-shell nanostructures during co-sputtering process, which exhibit high strength, large plasticity and good thermal stability as measured by compression test at various temperatures [28]. Crystalline-amorphous nanolaminates [19,29-31] usually display high strength and measurable plasticity under compression test normal to interface plane or tension parallel to interface plane, however delamination and buckling happen when applying the inverse loading, showing both tension-compression asymmetric and anisotropic properties of nanocomposites, as well as low bonding/shear strength of interfaces [27–30].

In this study, Ni-SiOC nanocomposite was synthesized by cosputtering Ni (99.995%), SiC (99.5%) and SiO₂ (99.995%) targets by using AJA ATC-2000F sputtering system with a base pressure of $\sim\!9.8\times10^{-6}$ Pa. The nominal content of Ni is about 75 at.% which was measured by energy dispersive X-ray spectroscopy analysis in transmission electron microscope (TEM) equipped with a quad Super-X detector. The as-deposited Ni-SiOC nanocomposite was then annealed at 600 °C and 800 °C under vacuum circumstance for 1 hour to further tune their microstructures. Ni-SiOC nanocomposites developed two

E-mail address: jianwang@unl.edu (J. Wang).

 $^{^{\}ast}$ Corresponding author.

B. Wei et al. Scripta Materialia 223 (2023) 115103

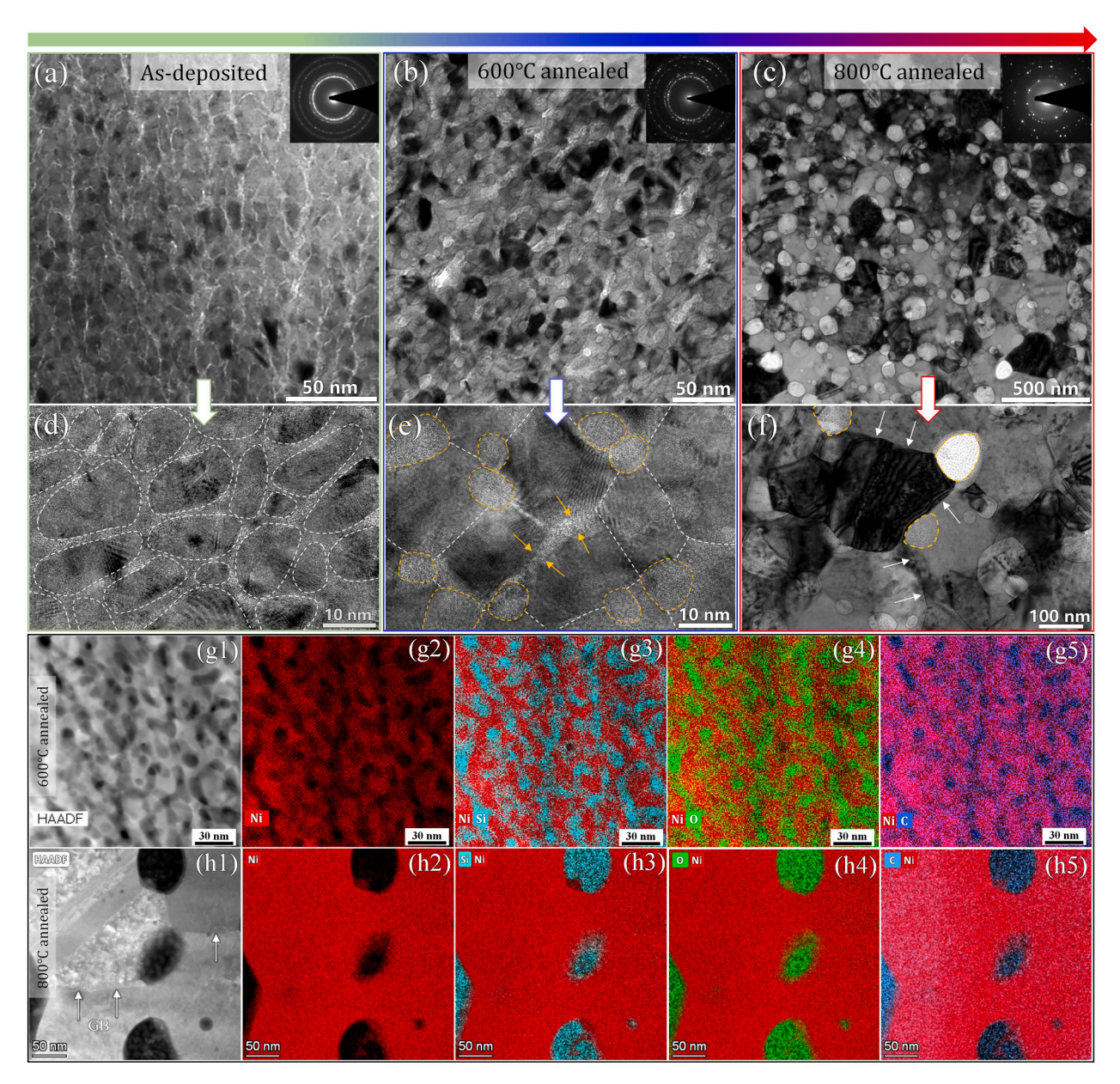


Fig. 1. TEM bright field images and corresponding electron diffraction patterns of Ni-SiOC nanocomposites: (a) as-deposited, (b) 600 °C annealed and (c) 800 °C annealed; HRTEM observation and enlarged TEM bright field images of Ni-SiOC nanocomposites: (d) as-deposited, (e) 600 °C annealed and (f) 800 °C annealed; (g) STEM-Mapping of 600 °C annealed Ni-SiOC nanocomposite; (h) STEM-Mapping of 800 °C annealed Ni-SiOC nanocomposite.

characteristic microstructures: core (crystalline Ni)-shell (amorphous SiOC) nanostructures and submicron-grained Ni containing amorphous ceramic SiOC particles. This offers the chance to reveal the effects of characteristic structure and bonding strength between Ni and amorphous ceramic SiOC on the mechanical behaviour of Ni-SiOC nanocomposites under different loading conditions. *In-situ* SEM compression and tension tests were thus conducted to study the tension-compression mechanical behaviour of Ni-SiOC nanocomposites with respect to these two characteristic microstructures. *In-situ* SEM compression test showed that both Ni-SiOC nanocomposites reveal high strength and plastic flow stability, while very limited plasticity was observed under their tension tests. The corresponding deformation and fracture mechanisms were discussed based on microscopy characterization after deformation.

Fig. 1 show the TEM microstructure of as-deposited Ni-SiOC nanocomposite and corresponding microstructural evolution after 600 °C and 800 °C annealing. The as-deposited sample (Fig. 1a) show obvious coreshell structure with amorphous ceramic SiOC along GBs of NC Ni (~13

nm). After high temperature annealing, both Ni and amorphous SiOC grew, which is about 22 nm (Ni) and 9 nm (SiOC) in 600 °C annealed sample (Fig. 1b), 220 nm (Ni) and 110 nm (SiOC) in 800 °C annealed sample (Fig. 1c). Fig. 1d-f show HRTEM observation and enlarged TEM image of Ni-SiOC nanocomposites corresponding to these three states. Note that except for SiOC nanoparticles, amorphous SiOC phase remained along GB of NC Ni in 600 °C annealed sample (marked by yellow arrow in Fig. 1e). We therefore also treated it as a specific coreshell structure. In contrast to 600 °C annealed sample, amorphous SiOC particles in 800 °C annealed sample were mainly distributed at triple junction of sub-micron sized Ni grains, and most of GBs are clean without decoration of SiOC phase (marked by white arrow in Fig. 1f). These two characteristic microstructures were further verified by EDX STEM-Mapping as shown in Fig. 1g and h. Note that no amorphous elements (Si, O and C) segregation at GB was observed in 800 °C annealed Ni-SiOC nanocomposite. Also, no mixing of Ni and amorphous elements existed, thus no intermetallic compounds are produced after high

B. Wei et al. Scripta Materialia 223 (2023) 115103

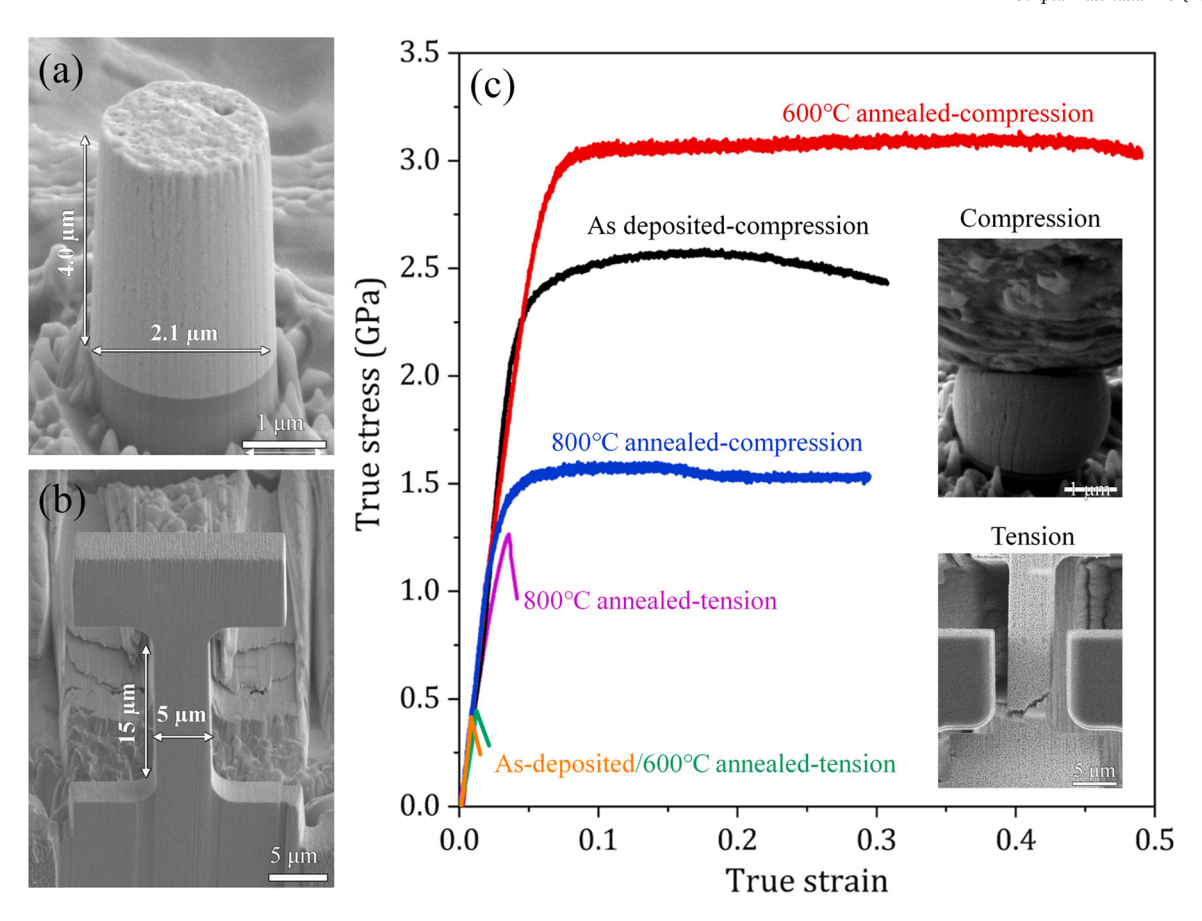


Fig. 2. (a) SEM image of cylindrical micropillar for *in-situ* compression test; (b) SEM image of dog-bone shaped micropillar for *in-situ* tension test; (c) True stress-strain curves of Ni-SiOC nanocomposites with respect to different microstructures and loadings.

temperature annealing.

In-situ SEM compression and tension tests were performed to study the asymmetric mechanical behaviours of Ni-SiOC nanocomposites by using a Hysitron PI85 PicoIndenter under a displacement-control mode at strain rate of 10^{-3} s $^{-1}$. Note that the sample size for *in-situ* mechanical test was reported to have significant impact on the mechanical behaviour of the testing materials [32,33]. For example, smaller is stronger, and plasticity or even ductility was observed in brittle materials when the sample size is reduced to nanoscale or submicron scale [34,35]. To diminish the size effect, micron-scaled cylindrical and dog-bone shaped micropillars that contains more than hundreds or thousands of constituents were fabricated by focused ion beam (FIB) using an FEI Helios Nanolab 660 dual beam system. Great care was taken to reduce the taper angle effect by using low milling current (10-40 pA). Transmission electron microscope (TEM) and scanning TEM (STEM) characterizations were performed using an FEI Tecnai Osiris and Talos F200X TEM operated at 200 kV. Cross-sectional TEM samples before and after deformation were prepared by FIB lift-out technique. Low energy Ar⁺ ion milling at 2 kV for 1–5 mins was conducted to remove surface pollution on TEM samples by using Gatan PIPS II system.

Fig. 2a and b show representative SEM images of the cylindrical and dog-bone shaped micropillars, respectively. The diameter of cylindrical micropillar for compression test is about 2–3 μ m. For the tensile sample, the gauge length is about 15 μ m and width is 5 μ m. This dimension is large enough to diminish size effect for *in-situ* mechanical test of Ni-SiOC nanocomposites. Fig. 2c present true stress-strain curves of Ni-SiOC nanocomposites. Compressive true stress-strain curves show that all Ni-SiOC nanocomposites exhibit high strength and good plastic flow stability. For example, the 600 °C annealed sample exhibit high flow strength of \sim 3 GPa and large plasticity up to 50%, showing both improved strength and plasticity compared to the as-deposited sample

(2.5 GPa flow strength, 35% plastic strain). The 800 °C annealed sample present obviously decreased flow strength (1.5 GPa), which should be ascribed to the increased grain size of Ni after annealing. In addition, no obvious strain hardening behaviour was observed. In contrast to compression test, these two characteristic structures show limited plasticity under tension test. The as-deposited and 600 °C annealed samples with core-shell structure reveal brittle behaviour at very low tensile stress (< 500 MPa). The 800 °C annealed sample with submicrongrained structure and amorphous ceramic SiOC particles present comparable strength of $\sim\!1.3$ GPa to that of compression test but very low ductility (<3%).

In-situ mechanical tests reveal obvious tension-compression asymmetric mechanical behaviour of the Ni-SiOC nanocomposites. To reveal underlying mechanisms, the microstructures of Ni-SiOC nanocomposites after deformation were characterized. Fig. 3 show the deformed microstructure after compression test. SEM snapshots of micropillars during compression (Fig. 3a-c) reveal high plastic flow stability of Ni-SiOC nanocomposites. In 800 °C annealed sample (Fig. 3c), clear codeformation between Ni and amorphous SiOC particles was identified, where amorphous particles were deformed by direct plastic flow (green arrow) and rotation (red arrow). Fig. 3d and e show TEM and HRTEM characterization of the 600 °C annealed sample, in which the amorphous SiOC phases were compressed into stripes and no interface decohesion existed, implying good deformation compatibility between NC Ni and amorphous SiOC ceramic. Stacking faults were frequently observed in NC Ni, indicating that plastic deformation of NC Ni was dominated by partial dislocation motion. Due to the fine grain size, dislocation was difficult to accumulate inside Ni grain, no obvious strain hardening behaviour was thus observed in true compression stress-strain curve (Fig. 2c). Fig. 3f and g reveal TEM and HRTEM characterization of the 800 °C annealed sample. Except for the shape change of amorphous

Scripta Materialia 223 (2023) 115103

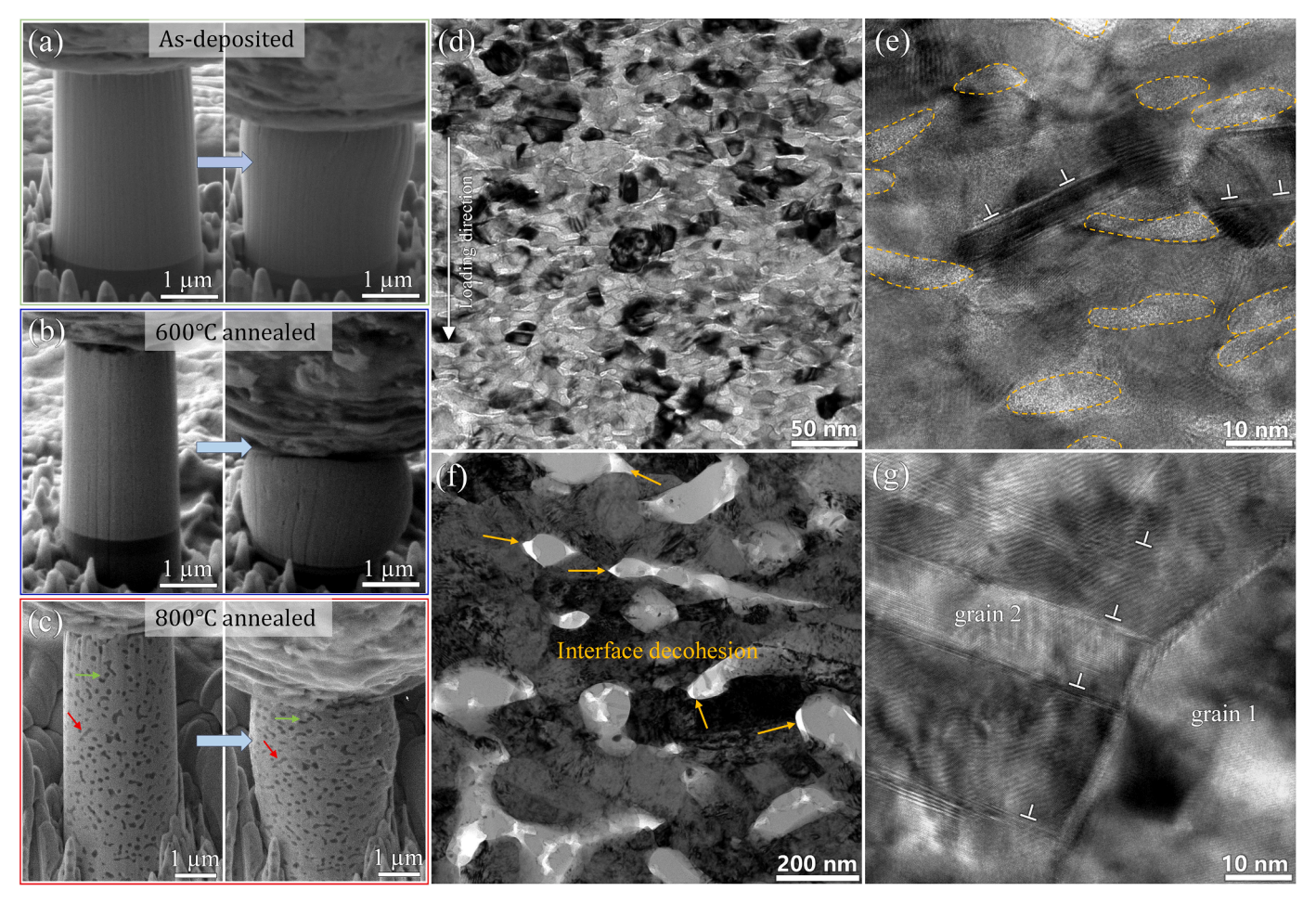


Fig. 3. SEM snapshots of micropillars during *in-situ* compression test: (a) as-deposited, (b) 600 °C annealed and (c) 800 °C annealed; (d-e) TEM characterization of the 600 °C annealed Ni-SiOC nanocomposite after compression test.

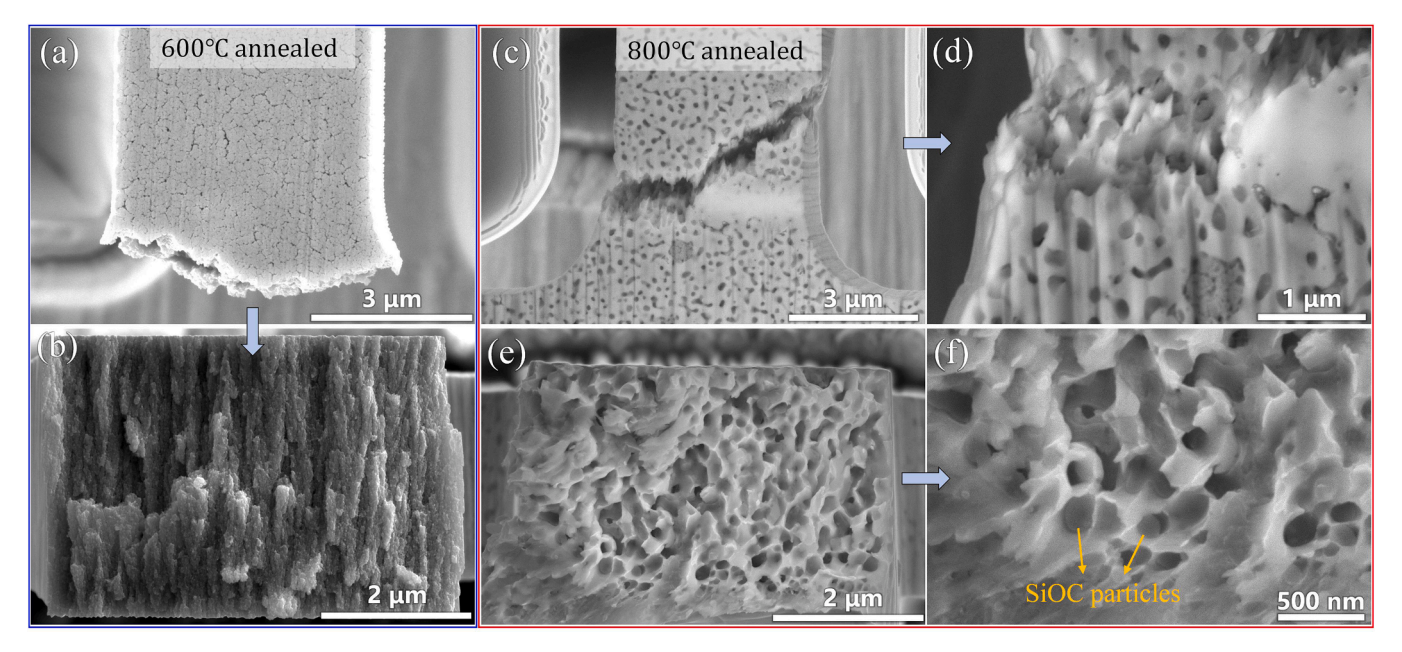


Fig. 4. (a-b) SEM images of fracture surfaces taken from top and cross-sectional surfaces of the 600 °C annealed sample after tension test; (c-f) SEM images of fracture surfaces taken from top and cross-sectional surfaces of the 800 °C annealed sample after tension test.

B. Wei et al. Scripta Materialia 223 (2023) 115103

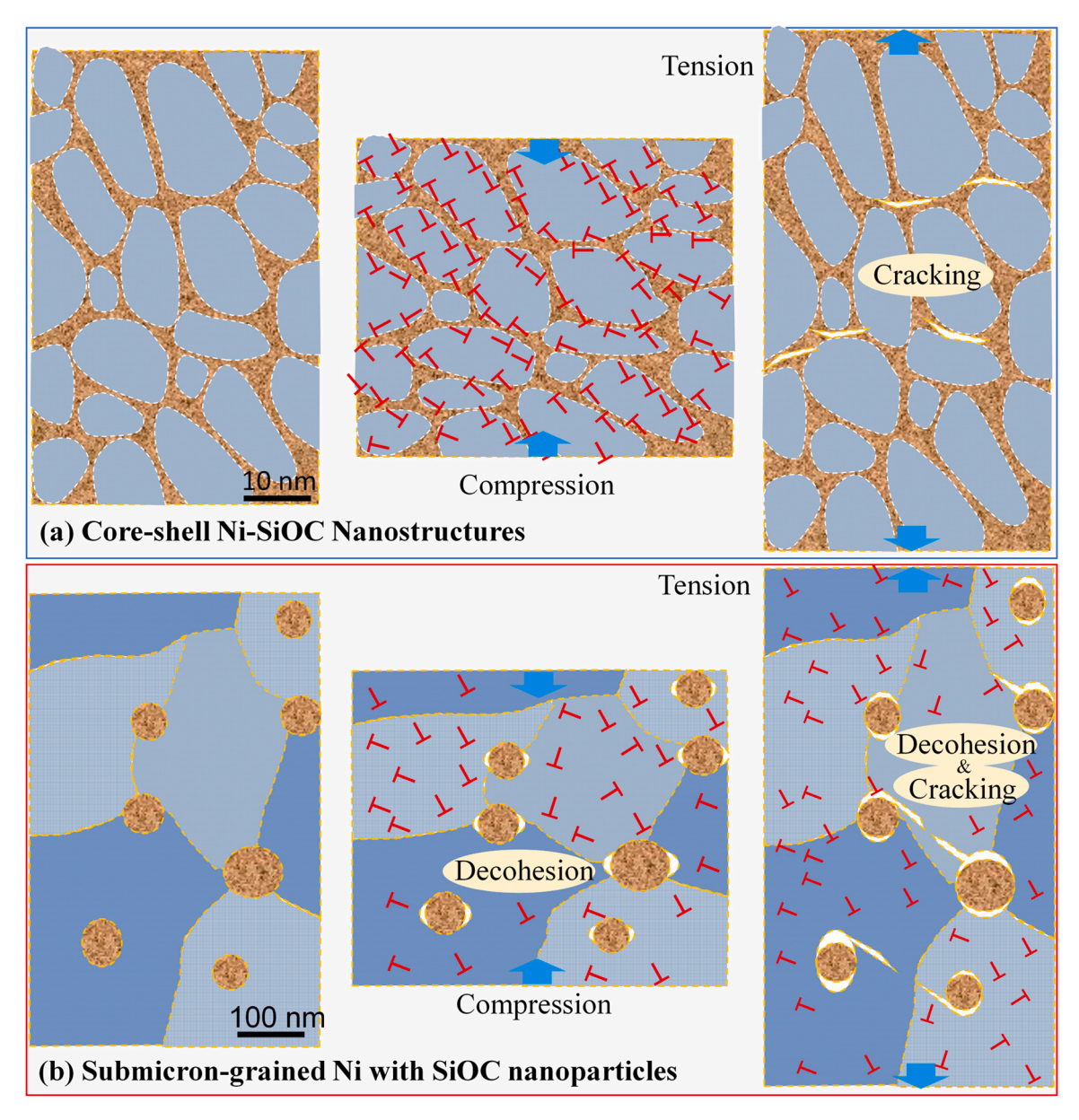


Fig. 5. (a) Schematic diagram of deformation mechanism for core-shell structure (as-deposited and 600 °C annealed Ni-SiOC nanocomposite); (b) Schematic diagram of deformation mechanism for sub-micron sized Ni containing amorphous ceramic SiOC particles (800 °C annealed Ni-SiOC nanocomposite).

SiOC particles by deformation, local interface decohesion between Ni and SiOC phase were observed (marked by yellow arrows in Fig. 3f). This is supposed to act as a softening behaviour that could counteract the strain hardening produced by dislocation storage in submicron-grained Ni. Correspondingly, the true compression stress-strain also do not show obvious hardening behaviour. Fig. 3g show a representative HRTEM image of Ni grain boundary after deformation. As can be seen that numerous stacking faults were stopped by the grain boundary and no crack or decohesion exists.

Fig. 4 present the SEM fracture surface of Ni-SiOC nanocomposites after tension test. The 600 °C annealed sample with core-shell structure exhibit clearly brittle facture surface as observed from both top and cross-sectional surfaces (Fig. 4a and b). The brittle behaviour should be ascribed to GB decohesion/cracking at amorphous SiOC grain boundary under very low tensile stress. This proves the weak interface bonding strength between Ni and amorphous SiOC phase. In contrast to the brittle fracture surface, 800 °C annealed sample show obvious ductile fracture surface with dimples (Fig. 4c-f). The dimple size is close to half the diameter of Ni grains. This implies that the plastic deformation was

mainly proceeded in Ni. Moreover, clear interface decohesion between Ni and amorphous SiOC particles were observed, implying that interface decohesion was easily occurred due to local stress concentration and low interface bonding strength, leading to low ductility.

The apparent tension-compression asymmetric mechanical behaviour of Ni-SiOC nanocomposites should be ascribed to their characteristic microstructure and interface strength (shear strength and bonding strength). Amorphous SiOC phase co-deformed with crystal Ni under compressive loading, while limited ductility and even brittle behaviour was observed under tension loading. Corresponding deformation mechanisms are rationalized as follows and illustrated in Fig. 5. The weak tensile strength and poor tensile plasticity could be ascribed to low bonding strength between metallic Ni and amorphous SiOC ceramic. For the core-shell structure (600 °C annealed sample) with amorphous phase existed along GB, GB decohesion may occur at very low tensile stress if the bonding strength is low, leading to cracking along the amorphous GBs (Fig. 5a). For the sub-micron sized Ni containing amorphous ceramic SiOC particles (800 °C annealed sample), high tensile strength is remained because plastic deformation is mainly accommodated by

dislocations in submicron Ni grains (Fig. 5b). More importantly, the GB is relatively clean and GB decohesion thus does not happen. However, plastic deformation incompatibility between soft submicron grained Ni and hard amorphous SiOC ceramic causes interface decohesion (Fig. 5b) due to the low interface bonding strength between Ni and SiOC particles. As a result, the accumulated dislocations in soft phase (Ni) are relaxed due to the created free surfaces, weakening the strain hardening capability, transferring the loading to Al matrix and leading to cracking in Al matrix and low ductility (Fig. 5b). However, under compressive loading the low interface bonding strength will facilitate the reaction and rearrangement of lattice dislocations blocked by the crystal-amorphous interfaces. For core-shell nanostructures, such dislocation mechanisms at weak interfaces promot plastic co-deformation between Ni nanograins and amorphous shells and prevent shear localization, thus leading to great plastic flow stability. For submicron-grained Ni-SiOC composites, such dislocation mechanisms relax plastic deformation incompatibility between soft submicron grained Ni and hard amorphous SiOC ceramic to interface decohesion, weakening strain hardening capability.

In summary, in-situ micromechanical tests of Ni-SiOC nanocomposites with two characteristic microstructures reveal significant tension-compression mechanical asymmetric mechanical response. The results will demonstrate the effect of interface strength and deformation incompatibility associated the microstructure on the tensioncompression asymmetry. Plasticity is the ability of a solid material to undergo plastic deformation without fracture, which is usually measured under compressive stress because localized deformation (necking) does not occur under such a loading condition. Ductility is defined as the uniform elongation measured from tensile test. High plasticity is just a prerequisite for high ductility but not guarantee high ductility. To achieve high ductility, materials should also exhibit high strain hardening behaviour that can effectively postpone necking behaviour and inhibit strain localization. In compressive stress-strain curves of Ni-SiOC nanocomposites, no obvious strain hardening behaviour was observed, implying the easily occurrence of strain localization. More importantly, for a composite material or alloy that contain a second phase, interface shear strength and bonding strengths are crucial to maintain plasticity and ductility of materials. Once plastic deformation incompatibility develops across the interfaces, low shear strength of interfaces will facilitate dislocations deflection along the interfaces, causing interface shear. Localized shear along the interfaces will promote emission of dislocations from the sheared interface into the matrix, facilitating the formation of interface decohesion, as illustrated in Fig. 5. Under tensile loading, localized shear will further promote cracking initiation, leading to low ductility. In addition, interface bonding strength determines the maximum tension strength between Ni matrix and amorphous SiOC ceramic. Thus, the weak bonding strength and obvious deformation incompatibility between sub-micron sized Ni and amorphous ceramic SiOC lead to interface decohesion at low strain, producing low ductility. Present study suggests that good interface strength, strain hardening and deformation compatibility between different phases are key factors to remain good ductility.

Author statement

Wei and Wu synthesized materials and performed in situ micromechanical tests and TEM characterization; Wei, Wang prepared the manuscript. All authors commented the manuscript.

Declaration of competing interest

The authors declare that they have no known competing financial interests or personal relationships that could have appeared to influence the work reported in this paper.

Acknowledgments

The research was financially supported by the US National Science Foundation (NSF) (CMMI- 2132336/2132383), and performed in the Nebraska center for Materials and Nanoscience which is supported by the National Science Foundation under Award ECCS: 1542182 and the Nebraska Research Initiative.

References

- H. Wu, G. Fan, An overview of tailoring strain delocalization for strength-ductility synergy, Prog. Mater. Sci. 113 (2020), 100675.
- [2] L.G. Sun, G. Wu, Q. Wang, J. Lu, Nanostructural metallic materials: structures and mechanical properties, Mater. Today 38 (2020) 114–135.
- [3] Y.T. Zhu, X.L. Wu, Ductility and plasticity of nanostructured metals: differences and issues, Mater. Today Nano 2 (2018) 15–20.
- [4] M.A. Meyers, A. Mishra, D.J. Benson, Mechanical properties of nanocrystalline materials, Prog. Mater. Sci. 51 (4) (2006) 427–556.
- [5] C.S. Pande, K.P. Cooper, Nanomechanics of Hall–Petch relationship in nanocrystalline materials, Prog. Mater. Sci. 54 (6) (2009) 689–706.
- [6] D. Wolf, V. Yamakov, S.R. Phillpot, A. Mukherjee, H. Gleiter, Deformation of nanocrystalline materials by molecular-dynamics simulation: relationship to experiments, Acta Mater. 53 (1) (2005) 1–40.
- [7] Z. Wang, W. Lu, H. Zhao, C.H. Liebscher, J. He, D. Ponge, D. Raabe, Z. Li, Ultrastrong lightweight compositionally complex steels via dual-nanoprecipitation, Sci. Adv. 6 (46) (2020) eaba9543.
- [8] T. Yang, Y.L. Zhao, Y. Tong, Z.B. Jiao, J. Wei, J.X. Cai, X.D. Han, D. Chen, A. Hu, J. J. Kai, K. Lu, Y. Liu, C.T. Liu, Multicomponent intermetallic nanoparticles and superb mechanical behaviors of complex alloys, Science 362 (6417) (2018) 933–937
- [9] J. Du, S. Jiang, P. Cao, C. Xu, Y. Wu, H. Chen, E. Fu, Z. Lu, Superior radiation tolerance via reversible disordering-ordering transition of coherent superlattices, Nat. Mater. (2022).
- [10] Z.X. Wu, Y.W. Zhang, M.H. Jhon, D.J. Srolovitz, Anatomy of nanomaterial deformation: grain boundary sliding, plasticity and cavitation in nanocrystalline Ni, Acta Mater. 61 (15) (2013) 5807–5820.
- [11] S.D. Antolovich, R.W. Armstrong, Plastic strain localization in metals: origins and consequences, Prog. Mater. Sci. 59 (2014) 1–160.
- [12] Y.M. Wang, E. Ma, Strain hardening, strain rate sensitivity, and ductility of nanostructured metals, Mater. Sci. Eng. A 375-377 (2004) 46–52.
- [13] J. Schiøtz, F.D. Di Tolla, K.W. Jacobsen, Softening of nanocrystalline metals at very small grain sizes, Nature 391 (6667) (1998) 561–563.
- [14] B. Wang, M.T. Alam, M.A. Haque, Grain growth in nanocrystalline nickel films at low temperature and stress, Scr. Mater. 71 (2014) 1–4.
- [15] Y. Zhang, G.J. Tucker, J.R. Trelewicz, Stress-assisted grain growth in nanocrystalline metals: grain boundary mediated mechanisms and stabilization through alloying, Acta Mater. 131 (2017) 39–47.
- [16] Q. Wei, D. Jia, K.T. Ramesh, E. Ma, Evolution and microstructure of shear bands in nanostructured Fe, Appl. Phys. Lett. 81 (7) (2002) 1240–1242.
- [17] E. Ma, Instabilities and ductility of nanocrystalline and ultrafine-grained metals, Scr. Mater. 49 (7) (2003) 663–668.
- [18] M.Y. Gutkin, K.N. Mikaelyan, I.A. Ovid'ko, Grain growth and collective migration of grain boundaries during plastic deformation of nanocrystalline materials, Phys. Solid State 50 (7) (2008) 1266–1279.
- [19] L. Bai, B. Wei, J. Wang, K. Ming, S. Zheng, J. Wang, High strength and thermal stability of core-shell Fe-SiOC nanocolumnar composites, Scr. Mater. 219 (2022), 114885
- [20] P. Sathiyamoorthi, J. Basu, S. Kashyap, K.G. Pradeep, R.S. Kottada, Thermal stability and grain boundary strengthening in ultrafine-grained CoCrFeNi high entropy alloy composite, Mater. Des. 134 (2017) 426–433.
- [21] P.R. Cantwell, M. Tang, S.J. Dillon, J. Luo, G.S. Rohrer, M.P. Harmer, Grain boundary complexions, Acta Mater. 62 (2014) 1–48.
- [22] W. Sun, J. Luo, Y.Y. Chan, J.H. Luan, X.-S. Yang, An extraordinary-performance gradient nanostructured Hadfield manganese steel containing multi-phase nanocrystalline-amorphous core-shell surface layer by laser surface processing, J. Mater. Sci. Technol. 134 (2023) 209–222.
- [23] Y. Wang, J. Li, A.V. Hamza, T.W. Barbee, Ductile crystalline-amorphous nanolaminates, Proc. Natl. Acad. Sci. 104 (27) (2007) 11155–11160.
- [24] G. Wu, S. Balachandran, B. Gault, W. Xia, C. Liu, Z. Rao, Y. Wei, S. Liu, J. Lu, M. Herbig, W. Lu, G. Dehm, Z. Li, D. Raabe, Crystal–glass high-entropy nanocomposites with near theoretical compressive strength and large deformability, Adv. Mater. 32 (34) (2020), 2002619.
- [25] G. Wu, C. Liu, L. Sun, Q. Wang, B. Sun, B. Han, J.-.J. Kai, J. Luan, C.T. Liu, K. Cao, Y. Lu, L. Cheng, J. Lu, Hierarchical nanostructured aluminum alloy with ultrahigh strength and large plasticity, Nat. Commun. 10 (1) (2019) 5099.
- [26] K. Ming, Z. Zhu, W. Zhu, B. Fang, B. Wei, P.K. Liaw, X. Wei, J. Wang, S. Zheng, Enhancing strength and ductility via crystalline-amorphous nanoarchitectures in TiZr-based alloys, Sci. Adv. 8 (10) (2022) eabm2884.
- [27] F.C. Li, T. Liu, J.Y. Zhang, S. Shuang, Q. Wang, A.D. Wang, J.G. Wang, Y. Yang, Amorphous–nanocrystalline alloys: fabrication, properties, and applications, Mater. Today Adv. 4 (2019), 100027.

- [28] B. Wei, W. Wu, D. Xie, M. Nastasi, J. Wang, Strength, plasticity, thermal stability and strain rate sensitivity of nanograined nickel with amorphous ceramic grain boundaries, Acta Mater. 212 (2021), 116918.
- [29] T. Müller, A. Bachmaier, R. Konetschnik, T. Schöberl, R. Pippan, Mechanical properties of electrodeposited amorphous/crystalline multilayer structures in the Fe-P system, Mater. Sci. Eng. A 715 (2018) 83–91.
- [30] G. Plummer, H. Rathod, A. Srivastava, M. Radovic, T. Ouisse, M. Yildizhan, P.O. Å. Persson, K. Lambrinou, M.W. Barsoum, G.J. Tucker, On the origin of kinking in layered crystalline solids, Mater. Today 43 (2021) 45–52.
- [31] Z. Fan, S. Xue, J. Wang, K.Y. Yu, H. Wang, X. Zhang, Unusual size dependent strengthening mechanisms of Cu/amorphous CuNb multilayers, Acta Mater. 120 (2016) 327–336.
- [32] J.R. Greer, J.T.M. De Hosson, Plasticity in small-sized metallic systems: intrinsic versus extrinsic size effect, Prog. Mater. Sci. 56 (6) (2011) 654–724.
- [33] V. Jayaram, Small-Scale Mechanical Testing, Annu. Rev. Mater. Res. 52 (2022).
- [34] G. Wu, J. Zhang, C. Liu, Q. Wang, J. Lu, Ductility of an ultrastrong glass-crystal nano-dual-phase alloy in sub-micron, Scr. Mater. 183 (2020) 17–21.
- [35] J. Luo, J. Wang, E. Bitzek, J.Y. Huang, H. Zheng, L. Tong, Q. Yang, J. Li, S.X. Mao, Size-dependent brittle-to-ductile transition in silica glass nanofibers, Nano Lett. 16 (1) (2016) 105–113.